Aerospace Science and Technology 155 (2024) 109629

Contents lists available at ScienceDirect

Aerospace Science and Technology

journal homepage: www.elsevier.com/locate/aescte

Multipolar expansion for aircraft noise equivalent sources

Giorgio Palma [a,b,*], Lorenzo Burghignoli [b], Caterina Poggi [b], Jacopo Serafini [b]

[a] National Research Council-Institute of Marine Engineering, CNR-INM, Via di Vallerano, 139, Roma, 00128, Italy
[b] Department of Civil, Computational Science and Aeronautical Technologies Engineering, Roma Tre University, Via Vito Volterra, 62, Roma, 00146, Italy

ARTICLE INFO

Communicated by Antonio Filippone

Keywords:
Aviation noise
Reduced-order modeling
Analytical expansion
Physics-informed regression

ABSTRACT

Noise generated by aviation poses serious threats to its future development. Noise abatement is pursued by reducing noise at the source and using correct operation practices and farsighted land planning. Since noise evaluation is a computationally demanding process, developing fast techniques is crucial for that noise abatement effort. Widely used approaches separate near-field noise from far-field noise, using the optical analogy or other simplified techniques to radiate to the ground the noise evaluated in the near-field by high-fidelity models, including atmospheric and geographic effects. Here, we propose a multipolar expansion to define equivalent noise sources that can be quickly evaluated to simulate the perceived noise also in proximity of the source. This gives many advantages, such as introducing atmospheric effects closer to the source and using equivalent engine sources in fuselage scattering problems. The expansion is tested against numerical and experimental test cases of aeronautical interest. The results show that the expansion effectively reproduces noise at different distances than that used to train the equivalent source. When the emitted noise is dominated by rotary sources, the method correctly reproduces the amplitude but not the phase of the signals.

1. Introduction

Noise exposure, especially at night, has been widely demonstrated to threaten public health because it creates physical and psychological stress, causes cognitive impairment in children, and can negatively affect the cardiovascular and metabolic systems [1]. In addition, it reduces productivity and interferes with communication and concentration. Thus, the EU (like many other governments) has set an ambitious plan to reduce the population exposed to harmful noise levels to zero [2–4]. At the same time, although aviation noise is a fairly localized problem (mainly in the proximity of airports and flight routes), noise is one of the main factors limiting aviation expansion in terms of airport growth and number of operations. Indeed, it is necessary to enforce noise limits in the areas surrounding airports, time limits to operations, and careful land use planning. International Civil Aviation Organization (ICAO) has defined the Balanced Approach to Aircraft Noise Management [5], which envisages four main ways to reduce noise nuisance. i) reduction of noise at source; ii) land use planning and management; iii) noise abatement operational procedures; iv) operating restrictions. The first point concerns the technological improvement in aircraft, mainly focused on reducing engine noise. EASA and FAA constantly update the certification requirements, and the governments set taxes to be paid by operators depending on the noise emitted in each operation. This approach encourages the manufacturer to reduce noise, producing aircraft with lower operating costs. Although great results have been achieved in the last decades, with a reduction of about 30 EPNdB at certification points in 60 years for an average transport aircraft, see Fig. 1 [6], the other three points are essential to achieve the mentioned ambitious goals despite the expected aviation growth. This is even more true since noise abatement at the source has almost reached a plateau that requires complex and groundbreaking innovation to overcome. The last three points require the evaluation of perceived noise on the ground, a nontrivial task greatly eased by using computational tools in conjunction with (or in place of) experimental testing. The first point also requires this evaluation, although only instrumentally for the evaluation of noise on certification points. Unfortunately, the accurate evaluation of the noise footprint of an aircraft operation is a multiphysics problem that involves many disciplines and scientific problems, like the simulation of generated noise by the engines and airframe and its propagation through a non-uniform medium, the atmosphere, with the inclusion of

* Corresponding author at: Department of Civil, Computational Science and Aeronautical Technologies Engineering, Roma Tre University, Via Vito Volterra, 62, Roma, 00146, Italy.
E-mail addresses: giorgio.palma@cnr.it (G. Palma), lorenzo.burghignoli@uniroma3.it (L. Burghignoli), caterina.poggi@uniroma3.it (C. Poggi), jacopo.serafini@uniroma3.it (J. Serafini).

https://doi.org/10.1016/j.ast.2024.109629
Received 6 March 2024; Received in revised form 20 September 2024; Accepted 24 September 2024
Available online 30 September 2024

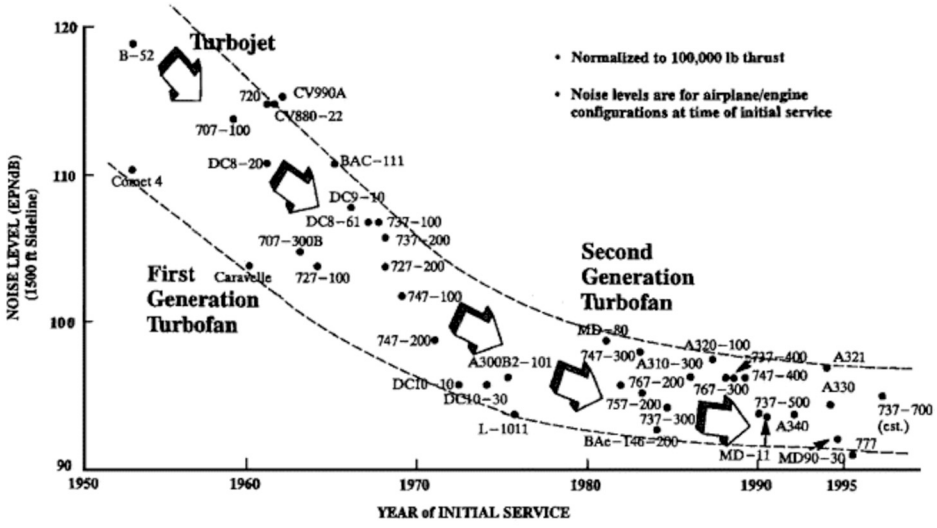

Fig. 1. Progress in aircraft noise reduction, reused with permission from [6].

ground reflection effect. The analysis of sound generation and propagation is generally conceived as a two-step problem: the first consists of the characterization of the noise sources localized in the region closer to the body, the so-called near-field. Various numerical techniques, differing in accuracy and fidelity, can be applied here, including high-fidelity CFD / CAA solvers [7]. However, owing to the relevant computational cost associated with those solvers, they are usually applied when a limited number of evaluations are required. On the contrary, when multiple evaluation are required (i.e. optimization, complete procedure assessment including possible changes in the aircraft operational configuration), less computationally demanding mid-fidelity solvers are employed such as, for example, those based on integral formulations [8]. Once the near-field propagation is solved, the noise can be radiated in the far-field. In this second step, high-fidelity CFD approaches become unfeasible due to the domain extension, and alternative approaches based on the free-space Green's function method are generally used [9,10], such as the porous Ffwocs-Williams and Hawkings' equations, Kirchoff's method, or Lighthill's analogy. The limitation of these approaches is that they do not easily allow for including atmospheric effects in the calculations, which are relevant for long propagation distances. To overcome this limitation, the optic analogy [11] and the so-called ray-tracing methods [12,13] can be used since the assumption of sound traveling along monodimensional paths (rays) and pressure to decrease linearly with distance tends to be valid for high Helmholtz numbers, *i.e.*, the combination of frequency and the distance between source and observer, defining the so-called far-field region. This two-step procedure has the great advantage of significantly reducing the computational burden, which is mainly due to the near-field noise source characterization.

An alternative approach envisages the use of equivalent sources for noise prediction. Several names can be found in the literature that refer to it, all sharing the basic concept of using elementary point sources to reconstruct the radiated or acoustic field, whose intensities are obtained matching known acoustic pressures and/or velocities at some monitoring points typically defining the surfaces of the original radiating geometry. The method uses equivalent sources located inside or outside the domain for an exterior or interior acoustic problem, respectively. A review of the topic can be found in [14]. The number and location of the sources are typically not defined a priori and are parameters for the method. For example, in [15], the sound radiated from the exhaust of an aircraft propfan engine was modeled using a series of ring sources, placed not only in the exhaust section but ranging from the inside of the engine shroud to the domain enclosed by the hub of the setup. The sources approximately follow the geometry of the emitting and scattering surfaces, and the sources' intensities are found imposing the boundary conditions on the original body surfaces, defining a method that is closely related to the boundary elements method. Another example is that by [16], in which the position (discretized in a grid) of the equivalent sources is obtained in the solution process, along with their intensities. Therefore, the solution parameters are optimized for a minimum difference between the normal component of the original surface velocity and the normal component of the particle velocity produced by the substitute sources at the control points. The authors tested the use of monopoles and higher-order sources obtained as discrete distributions of closely placed monopoles, called discrete multipoles, showing that the latter have better performances, in particular, for higher frequencies. Notable is also the work of Treeby et al. [17], in which the authors developed a method to generate equivalent interior sources that reproduce some near-field measurement data, (*i.e.* satisfying Dirichlet boundary conditions at some monitoring points). The equivalent sources are then used to predict the ultrasonic field, including non-linearity and complex heterogeneous material properties, using time-domain full-wave models. The main advantage of the equivalent sources method relies on the method being meshless, using point sources only, inside or outside the original geometries. Therefore, once the source intensities are evaluated, no integral should be calculated for acoustic prediction. However, the main critical problem of this class of methods is that there is no general rule in terms of the number and position of equivalent sources, and, in addition, numerical instabilities from ill-conditioned linear systems may appear.

This paper proposes a novel approach for defining an equivalent noise source based on a multipolar expansion trained with experimental or numerical data. A training set of acoustic evaluations is used to retrieve the coefficients of the terms of the series (imposing the solution at those points can be interpreted as the imposition of Dirichlet boundary conditions at some monitoring points), obtaining a physics-informed regression of the data. Since higher-order poles bring information on complex noise propagation (*i.e.*, they represent a complete functional base), the source model can be used for noise propagation at distances both farther and nearer than the location of the original information at a tiny fraction of the computational cost of the commonly applied evaluation models. This aspect would be beneficial, *e.g.*, for the mentioned aviation noise propagation task, allowing to drastically reduce the distance up to where the use of high-fidelity solvers is needed. In addition, once obtained, the multipolar source model may also be used in combination with (full-wave) solvers capable of conveniently including effects of (possibly non-linear) propagation in non-uniform media [18–20,17]. The multipole expansion is defined in terms

of the increasing-order moments (dipoles, quadrupoles, octapoles, etc.) derived from the fundamental solution for the Helmholtz wave equation, resulting in a computationally efficient tool both in the training phase and in the noise evaluation. In fact, the time required for the evaluation of the coefficients of the expansion is negligible and corresponds to a pseudo-inversion of a relatively small matrix. Similarly, the reconstruction of the acoustic field generated by the multipoles is a simple matrix-vector multiplication, which makes this approach particularly appealing in the context of multidisciplinary conceptual design optimization, trajectory optimization, and online noise annoyance estimation, where computational efficiency is a crucial aspect. Numerical results show the capability of the method to capture the characteristics of complex acoustic fields generated in some aeronautical cases of interest, such as a helicopter in landing, a quadcopter in hovering, and an advancing propeller. Moreover, such a technique may be easily applied to unconventional configurations, for which the use of semi-empirical models suffers from the unavailability of historical data. However, like all the data-driven methods, the reliability of the results strongly depends on the quality of the training set in terms of both accuracy and size. In addition, it is found that, when the propagation of rotating sources dominates the noise field, the proposed method struggles to predict the phase of the signal while still fairly reproducing the noise levels and their variation with the observer position.

The article is organized as follows. Details on the methodology and multipolar expansion are given in Section 2. The multipolar expansion is then validated on an analytic test case that uses a combination of elementary point sources defining the acoustic field to be reproduced and tested on some benchmark of aeronautical interest in Section 3. Finally, the concluding remarks can be found in Section 4.

2. Methodology

This work proposes to approximate the reference acoustic field with a series of elementary sources from a multipolar linear expansion of arbitrary order:

$$p(\mathbf{x}) = \sum_{i=0}^{N} \mathcal{A}_i \cdot \mathcal{P}_i(\mathbf{x}) \tag{1}$$

where $\mathcal{A}_i$ and $\mathcal{P}_i$ are tensors of order i (*i.e.,* scalars for $i=0$, vectors for $i=1$, etc.) representing the coefficients and the basis functions of the expansion, respectively, and the dot operator represents the generalized inner product. The pole of order zero is defined as the elementary monopole source, *i.e.,* the fundamental solution for the Helmholtz wave equation, and the acoustic pressure field it produces is represented by:

$$\mathcal{P}_0(\mathbf{x}) = \frac{e^{-i\kappa r}}{4\pi r} \tag{2}$$

where $\kappa = \omega/c$ is the ratio between the angular frequency ω and the speed of sound c, $r = |\mathbf{x} - \mathbf{x}_0|$ is the amplitude of the vector $\mathbf{r} = \mathbf{x} - \mathbf{x}_0$, which is the distance vector between the observation point $\mathbf{x}$ and the position of the source $\mathbf{x_0}$. The pole of order 1 can be defined as the gradient of Eq. (2), and generalizing:

$$\mathcal{P}_{n+1}(\mathbf{x}) : \nabla \mathcal{P}_n(\mathbf{x}) \tag{3}$$

In cartesian coordinates, the components of the vector $\mathcal{P}_1$ represent the three orthogonal dipole sources aligned with the three spatial directions $\mathbf{e}_j$:

$$\mathcal{P}_{1_j}(\mathbf{x}) = \nabla \mathcal{P}_0 \cdot \mathbf{e}_j = -\frac{e^{-i\kappa r}}{4\pi r^2}(1 + i\kappa r)\left(\frac{\mathbf{r}}{r} \cdot \mathbf{e}_j\right) \tag{4}$$

Analogously, the term $\mathcal{P}_2$ represents the quadrupolar sources.

$$\mathcal{P}_{2_{j,k}}(\mathbf{x}) = \nabla \mathcal{P}_{1_j} \cdot \mathbf{e}_k \tag{5}$$

Two different kinds of terms arise depending on the direction e_k, which can be interpreted as the two forms of quadrupolar sources, namely the linear (for $j = k$) and lateral quadrupole (for $j \neq k$) [21].

$$\nabla \mathcal{P}_{1_j} \cdot \mathbf{e}_k = \begin{cases} \dfrac{e^{-i\kappa r}}{4\pi r^3}\left[3(1 + ir\kappa) - r^2\kappa^2\right]\left(\dfrac{\mathbf{r}}{r} \cdot \mathbf{e}_j\right)\left(\dfrac{\mathbf{r}}{r} \cdot \mathbf{e}_k\right), & j \neq k \\ \dfrac{e^{-i\kappa r}}{4\pi r^3}\left[-(1 + i\kappa r) + (3 + 3ir\kappa - r^2\kappa^2)\right]\left(\dfrac{\mathbf{r}}{r} \cdot \mathbf{e}_j\right)^2, & j = k \end{cases} \tag{6}$$

The tensor $\mathcal{P}_2$ benefits from symmetry properties; in cartesian coordinates, one needs to define only the six independent components out of the nine composing the tensor $\mathcal{P}_{2_{j,k}}$. The symmetry property generalizes for higher order tensors [22], and the independent components in a $\mathcal{R}^3$ space are defined in the number of

$$L_{\text{ind}} = \frac{(N + 3 - 1)!}{(3 - 1)!N!} \tag{7}$$

In fact, the terms whose indexes are permutations are not independent, so there is no need for their inclusion in the multipolar expansion.

Another interesting property can be exploited to reduce the number of the terms involved in the summation of Eq. (1). Summing the three linear quadrupoles (*i.e.* taking the trace of $\mathcal{P}_2$), one obtains a term proportional to the monopole source:

$$\sum_{j=1}^{3} \mathcal{P}_{2_{j,j}} = -\kappa^2 \mathcal{P}_0 \tag{8}$$

In general, this extends to higher orders, and each $\mathcal{P}_{N+2}$ comprises all the terms of the $\mathcal{P}_N$ tensor. This means that the summation in Eq. (1) can be reduced to the terms of the two highest orders since including lower order terms results in a linearly dependent basis. On the other hand, once one determines the $\mathcal{P}_{N+2}$ and $\mathcal{P}_{N+1}$ sources, it is always possible to obtain an equivalent set of linearly independent basis functions containing the sources of lower orders and removing the linearly dependent part from $\mathcal{P}_{N+2}$ and $\mathcal{P}_{N+1}$. In the case of quadrupoles, this means removing the algebraic average of the diagonal of the $\mathcal{A}_2$ tensor and adding the monopole term to the basis. Details of the generalization of this procedure are reported in Appendix A. Although unnecessary for the approximation of the reference field, the choice to include lower-order terms may be motivated by the common use of these sources to represent the acoustic field.

The method is equivalent to the use of spherical harmonics as a basis for the multipole expansion [23] ($e^{i\omega t}$ time convention):

$$p(r, \phi, \theta, \omega) = \sum_{l=0}^{N} \sum_{m=-l}^{l} A_{l,m} Y_{l,m}(\phi, \theta) h_l^{(2)}(\kappa r) \tag{9}$$

where $h_l^{(2)}(x)$ is l-th order spherical Hankel function of the second kind, providing the radial dependence of the solution and is defined as

$$h_l^{(2)}(x) = \sqrt{\frac{\pi}{2x}} H_{l+1/2}^{(2)}(x); \tag{10}$$

The real (Laplace's) spherical harmonics $Y_{l,m}$ of degree l and order m are a set of functions orthonormal over a sphere. They are the angular-depending portion of the solution of Laplace's operator in spherical coordinates, defined as

$$Y_{l,m} = \begin{cases} K_{l,m} \cos(m\phi) P_{l,m} \cos\theta & 0 \leq m \leq l \\ K_{l,m} \sin(|m|\phi) P_{l,|m|} \cos\theta & -l \leq m < 0 \end{cases} \quad l \in \mathcal{N}, \qquad K_{l,m} = \sqrt{\frac{(2l+1)(l - |m|)!}{4\pi(l + |m|)!}} \tag{11}$$

where $P_{l,m}$ is the associated Legendre polynomial and $K_{l,m}$ is a normalization constant. The spherical harmonic approach produces $L_{\text{ind}} =$

$\sum_{m=0}^{N} 2m+1$ independent functions. The one for $m=0$ corresponds to the monopole of Eq. (2), while $m=1$ produces the three dipoles of Eq. (4). For $m=2$ only five terms are involved in the expansion, while six terms arise from Eq. (6). This is not surprising, as the three linear quadrupoles and the monopole terms are linearly dependent, hence an orthogonal basis may elide one of the quadrupoles. In fact, each of the three linear quadrupolar terms can be obtained by linear combinations of the five terms of the spherical harmonics for $m=2$ and the term for $m=0$, while the remaining three lateral quadrupoles are directly mapped into one term of the spherical harmonic expansion (the relations hold analogously for higher polar orders and higher spherical harmonics). Multipolar expansion promises easy coupling with a classic geometric acoustic technique such as Geometrical Theory of Diffraction [24,25]. In the GTD framework, it is fundamental to define the diffraction coefficient for the specific acoustic source, as was done in [26] for the quadrupole point source. Using the same methodology, the diffraction coefficients may be derived for the higher-order sources for which the multipolar expansion provides amplitudes and phases.

The expansion in Eq. (1) contains N free parameters, namely the coefficients $\mathcal{A}_i$, adjustable to tune the equivalent sources to reproduce the acoustic field produced by the real sources. Some monitoring points where the acoustic field is known are defined. Those are subdivided into two sets: the first (called training set) contains Q points, whose acoustic measurements will be used to *train* the multipolar model; the second (test set) contains S points, whose acoustic pressures are only used to evaluate the performance of the equivalent source model at different locations not used in its training. To retrieve the coefficients $\mathcal{A}_i$ of the approximation in Eq. (1), the difference between the reference acoustic field and the field produced by the expansion is minimized in a mean square sense. Since the position of the equivalent sources is defined, this implies solving a linear system $\mathbf{Vz}=\mathbf{b}$, where $\mathbf{z}$ collects the M coefficients of $\mathcal{A}$. The vector $\mathbf{b}$ instead collects the values of the reference field at all the monitoring points Q, and the complex-valued pressures of the polar term M at the same monitoring points populate the columns of the $Q \times M$ matrix $\mathbf{V}$. The number of monitoring points in the training set limits the maximum order of the multipolar expansion as the system is solved using a Moore-Penrose pseudo-inverse (the condition $Q > L_{\text{ind}}(N)$ - ideally $Q >> L_{\text{ind}}(N)$ - has to be satisfied), namely:

$$\mathbf{z} = \mathbf{V}^{\dagger}\mathbf{b} = (\mathbf{V}^{*}\mathbf{V})^{-1}\mathbf{V}^{*}\mathbf{b} \tag{12}$$

where the superscript * indicates the complex conjugate operation.

2.1. Uniform mean flow effects

Some cases of aeronautical interest require including the free-stream velocity effect, which modifies both noise source characteristics and sound propagation. If the near-field noise is evaluated considering a uniform mean flow with small irrotational perturbations, the equivalent source may conveniently take into account the same effect using the Prandtl-Glauert transformation, which, in a frame of reference having the x-axis aligned with the free stream, reads

$$\begin{aligned} t_{pg} &= \beta t + \frac{M}{\beta c} x \\ x_{pg} &= \frac{x}{\beta} \\ y_{pg} &= y \\ z_{pg} &= z \end{aligned} \tag{13}$$

where M is the free stream Mach number and $\beta = \sqrt{(1-M^2)}$. It is well known that an acoustic problem in the presence of convection with solution p may be associated with a problem in a quiescent fluid with solution P such that, for a time-harmonic field, the following relations hold: $e^{i\omega t}p(x,y,z) = e^{i\Omega T}\mathrm{P}(x_{pg},y,z) = e^{i\omega t}e^{iKMx_{pg}}\mathrm{P}(x_{pg},y,z)$, with $\Omega = \omega/\beta$ and $K = \kappa/\beta$ and P solution of

$$\frac{\partial^2 \mathrm{P}}{\partial {x_{pg}}^2} + \frac{\partial^2 \mathrm{P}}{\partial y^2} + \frac{\partial^2 \mathrm{P}}{\partial z^2} + K^2 \mathrm{P} = 0 \tag{14}$$

Given the reference pressure field at some monitoring points, the coordinates of the virtual microphones are transformed with Eq. (13) to obtain the transformed position in which the acoustic pressure from the multipolar expansion is to be calculated. The terms of the expansion in Eq. (1) are evaluated using the transformed wavenumber K, and the phase delay $e^{iKMx_{pg}}$ is applied to the quiescent prediction to obtain the correct matrix V that accounts for the presence of flow to be compared with the reference pressure.

3. Numerical results

The proposed procedure is first validated against *ad hoc* generated noise data. The aim is twofold: i) to assess the capability of reproducing the signal in the training set and ii) to investigate the multipolar expansion generalization capability, namely extrapolating data on points not included in the training set. The validation against an analytical test case involved the use of a set of elementary sources of various polar orders with random amplitudes, phases, and positions to create the reference data at the monitoring points.

Once validated, the approach is applied to reproduce the noise radiated in three aeronautical cases: i) a quadcopter in hover; ii) a helicopter rotor in descent flight characterized by intense Blade-Vortex Interaction; iii) a propeller in forward flight.

The arrangement of the monitoring points (here on spheres of different radii, when available, or on a carpet) can be arbitrary. However, having points at multiple radial distances from the center of the polar expansion is beneficial when dealing with realistic acoustic fields to help the method capture the correct directivity propagation.

The results are shown in terms of the normalized relative root mean square error (RRMSE) [27]:

$$\mathrm{RRMSE} = \sqrt{\frac{\sum_{j=1}^{Q} |b_j - \hat{b}_j|^2}{\sum_{j=1}^{Q} |b_j|^2}} \tag{15}$$

where $\hat{b}_j$ is the acoustic field at the j-th monitoring point reproduced by the multipolar approximation and b_j is the value of the reference solution at the same point. When monitoring points are on multiple spheres, dedicated RRMSE_i

$$\mathrm{RRMSE}_i = \sqrt{\frac{\sum_{j=1}^{Q_i} |b_j - \hat{b}_j|^2}{\sum_{j=1}^{Q} |b_j|^2}} \tag{16}$$

are also evaluated, with Q_i considering only the points on the i-th sphere. In addition, the reference and reproduced Sound Pressure Levels (SPLs) in the microphones are shown as output to give a more immediate insight into the method's capabilities.

3.1. Analytic test case

As mentioned above, for the analytic test case, the reference acoustic field is produced by several elementary sources, namely monopoles, dipoles, and quadrupoles, with random position and complex-valued amplitude. The reference noise is evaluated on four spherical grids of 1369 points each, with radii $r_{m_1} = 10/k$, $r_{m_2} = 20/k$, $r_{m_3} = 30/k$, and $r_{m_4} = 100/k$. The elementary monopoles, dipoles, and quadrupoles producing the reference noise are placed inside a spherical region or radius $r_s = 0.5 r_{m_1}$. To enhance the anisotropy of the resulting field, the sources are forced to lay only in a quarter of the spherical region, as shown in

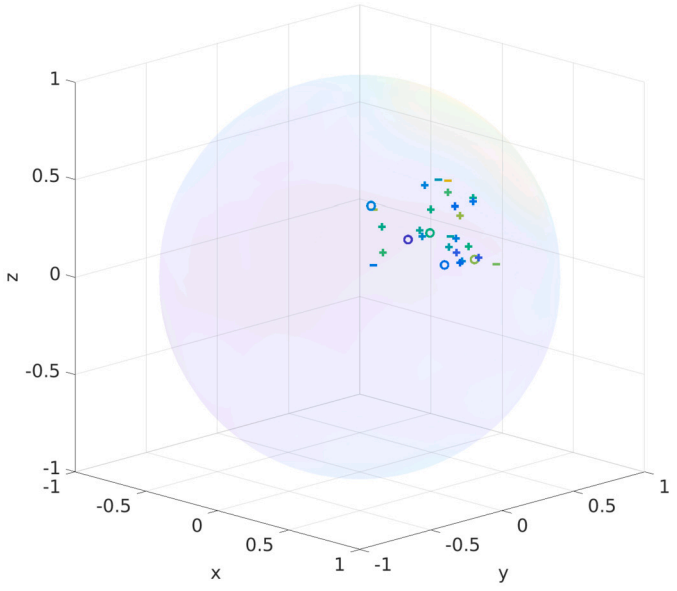

Fig. 2. Random positioning of elementary sources inside a sphere of radius $r_s = 0.5r_{m_1}$ with random complex-valued amplitudes for the analytic test case.

Fig. 2. The complex-valued amplitudes of the sources are randomly set between 0 and $1+1i$. The positions and amplitudes of the sources are resumed in the Supplementary Information.

Three subcases have been identified on the basis of which monitoring points are used in solving Eq. (12). In the first, the points lying on the three smaller spheres of radius $r_{m_{1-3}}$ are used; in the other two, only the points at r_{m_1} and r_{m_3} are used, respectively. The points lying on the other spheres are used as a test set, *i.e.* they are excluded from the vector $\mathbf{b}$ and matrix $\mathbf{V}^{\dagger}$. Fig. 3 shows the convergence trend for the mentioned cases when the order of the multipolar expansion is increased.

First, it can be observed that the reproduction error coherently decreases as the order of the multipolar expansion increases for all the tested training sets to less than 10^{-3} for the highest tested order $N = 20$. Furthermore, the reproduction capability of the model is similar in all the subcases, even though the rate of convergence of the RRMSE seems slightly better when including only the points on the sphere with radius $r_{m_3} = 30/k$ in the training set. The RRMSE_i of the points on the "test" spheres are all comparable to each other, confirming that the equivalent source can predict the acoustic pressure field in the whole domain. It is interesting to note that the RRMSE_i evaluated on the sphere in the close near-field, such as r_{m_1}, is typically higher than the others and, in general, the error appears to be lower moving the observation points in the far-field. This is somehow expected since the actual spatial distribution of the acoustic sources has a stronger impact in the near-field than in the far-field.

A qualitative comparison of the reproduction accuracy reached with $N = 11$ is shown in Fig. 4 in terms of SPL using points at r_{m_3} in the training set. The reference and reproduced fields are practically indistinguishable in all the addressed cases. Other figures for cases using points at r_{m_1} or $r_{m_{1-3}}$ are presented in the Supplementary Information.

3.1.1. Moving monopole

The method is then applied to the case of a moving source. This analysis aims to validate the proposed method in the presence of a uniform mean flow. In particular, it confirms the need to use moving sources (i.e., the sources evaluated in the PG-transformed space) instead of stationary ones to approximate the acoustic field generated by a moving body.

Here, the test case is a simple translating monopole, which can obviously be approximated with a single elementary source using the PG transformation, *i.e.*, using a zero-order expansion (see Fig. 5b). We also tested the approximation using the elementary sources in the physical (untransformed) space, but, as Fig. 5a shows, this approach fails to obtain a practical approximation of the noise source. The PG transformation only introduces a phase shift in the acoustic solution linked to the uniform stream convection velocity, and this appears to be fundamental for the expansion to capture the propagation characteristics of the reference field.

3.2. Aeronautical test cases

In this section, the proposed approach is applied to predict the noise emitted for realistic aeronautical cases. The analyzed cases are: i) a rotor in descent flight characterized by intense Blade-Vortex Interaction; ii) a quadcopter in hover; iii) a propeller in forward flight. The numerical database is obtained through an aerodynamic solver for potential and incompressible flows, followed by the application of the Farassat 1A boundary integral formulation for the evaluation of the noise field. Details on the numerical tools can be found in [28] and in [29] for the aerodynamic and acoustic formulations, respectively.

3.2.1. Landing helicopter rotor model

This test case is the noise footprint of the scaled-down baseline version (BL) of the hingeless four-bladed main rotor of the Bo-105 helicopter investigated in the HART II test campaign [30–32]. The rotor has a radius of $R = 2m$, a blade chord length of $c = 0.121$ m, a linear twist of $\theta_{tw} = -8$ deg / R, and rotates at $\Omega = 109.12$ rad/sec. The rotor is also subjected to a free stream (advance ratio equal to 0.15, angle of attack (shaft angle) of 5.3 deg) as in a descent flight. For further information on the rotor data, refer to the comprehensive study conducted in [33]. The numerical data set for the identification of the multipolar expansion consists of the numerical results presented in [34], where an internal comprehensive code has been successfully validated in terms of flowfield, blade airloads, aeroelastic response and noise emission against HART II data. In particular, the complex-valued acoustic pressure on a carpet of virtual microphones placed under the rotor and fuselage, at a distance of 2.215 m, is extracted for the first five multiples of the blade passing frequency (BPF) and used as reference pressure fields for the multipolar approximation.

First, Fig. 6 shows the normalized RRMSE as the multipolar expansion order increases. This convergence trend allows us to consider $N = 20$ as the converged value, due to the very low value of the error reached for all frequencies analyzed. Furthermore, for the first two BPFs, a satisfactory value of the error is also obtained for a lower-order multipolar expansion, namely $N = 11$. The good quality of the prediction obtained with $N = 20$ is demonstrated by the comparison between the reference and the reconstructed field shown in Fig. 7. In particular, the reconstructed acoustic fields using $N = 20$ are almost indistinguishable from the reference data for the first two BPF multiples, and negligible differences are present at higher frequencies (comparisons are shown in the Supplementary Information up to the fifth BPF multiple). In general, higher BPFs show multiple peaks in the directivity pattern, progressively narrower in space. Reproducing such pressure fields requires higher orders of the multipolar expansion to be used, as already pointed out by the convergence plot of Fig. 6.

It is important to highlight that, in this case, lying the microphones on a planar array, the multipolar expansion does not have information about the whole directivity, but only on a spherical sector. Hence, when interrogated on points outside the bounding box of the original data set, the model tries to extrapolate information with poor results. This limitation is well known for interpolative models and can be overcome using training points covering the entire spherical angle surrounding the sources of the expansion, which, however, were not available in this case.

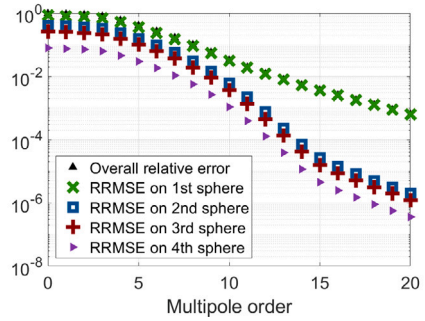

(a) Spheres of radii $r_{m_{1-3}}$ in the training set.

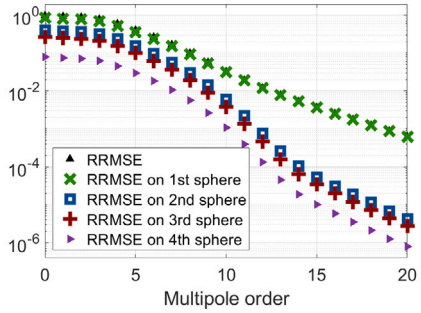

(b) Sphere of radius r_{m_1} in the training set.

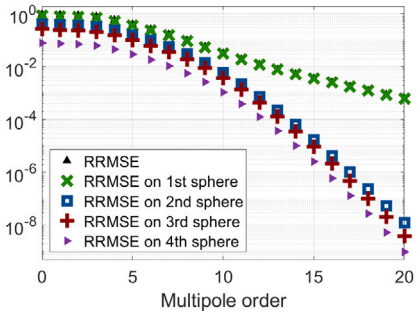

(c) Sphere of radius r_{m_3} in the training set.

Fig. 3. Convergence of the normalized RRMSE for the analytic test case.

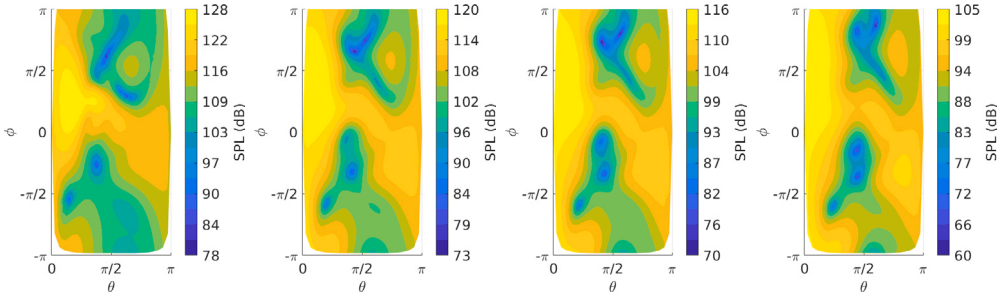

(a) Reference field, $r_{m_1} = 10/\kappa$

(b) Reference field, $r_{m_2} = 20/\kappa$

(c) Reference field, $r_{m_3} = 30/\kappa$

(d) Reference field, $r_{m_4} = 100/\kappa$

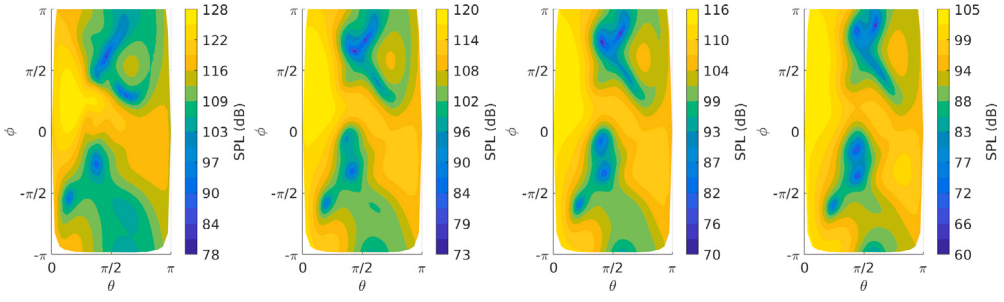

(e) Multipolar expansion, $r_{m_1} = 10/\kappa$

(f) Multipolar expansion, $r_{m_2} = 20/\kappa$

(g) Multipolar expansion, $r_{m_3} = 30/\kappa$

(h) Multipolar expansion, $r_{m_4} = 100/\kappa$

Fig. 4. Comparison between reference (Fig. 4a, Fig. 4b, Fig. 4c and Fig. 4d) and reconstructed (Fig. 4e, Fig. 4f, Fig. 4g and Fig. 4h) SPLs for the analytic test case at the four radial distances considered. Points at r_{m_3} used in the training set. (For interpretation of the colors in the figure(s), the reader is referred to the web version of this article.)

3.2.2. *Quadrotor in hovering*

The configuration herein investigated consists of a quadrotor whose main characteristics are reported in Table 1 (for further details on the configuration and the numerical modeling, see [35]).

The data set consists of the SPL at the first BPF, corresponding to $f = 152.79$ Hz, on three spheres centered in the center of gravity of the quadrotor and having radii equal to $r_{m_1} = 120$ m, $r_{m_2} = 140$ m, $r_{m_3} = 160$ m. Fig. 8 shows the convergence trend, in terms of normalized

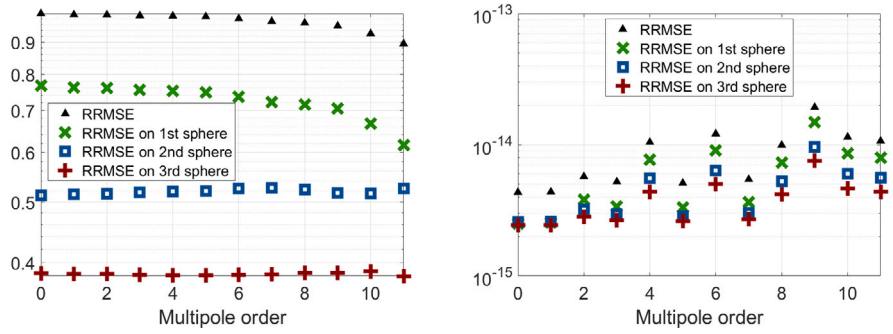

(a) Physical space multipolar expansion (b) PG transformed multipolar expansion

Fig. 5. Convergence of the normalized RRMSE, see Eq. (15), for the moving monopole test case. Fig. 5a shows the failure in reproducing the reference pressure field using fixed point sources even for high orders of the expansion, while, when using the P-G transformation approach to include the convection effect in the reproduced field, the expansion correctly catches the solution even including the first term only.

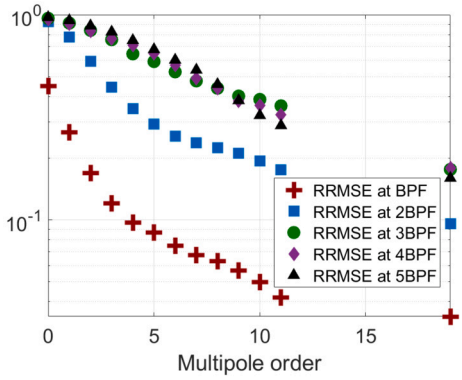

Fig. 6. Convergence of the normalized RRMSE for HART II test case for the first five BPF multiples (marked from first to fifth with crosses, squares, circles, diamonds, and triangles markers, respectively).

Table 1
Quadcopter characteristics.

Maximum take-off weight =	3000 kg	**Radius** =	4.0081 m
Blade counts =	3	**linear twist** =	12°
Mean chord =	0.2711 m	**Airfoil** =	VR7

RRMSE, when increasing the order of the multipolar expansion. The case in which all the points on the three spheres are used in the training set is addressed in Fig. 8a, while Fig. 8b and Fig. 8c show the trend of the error obtained using only the closest and the farthest sphere in the training set, respectively. When all the data are used to train the model (Fig. 8a), the normalized RRMSE over the three spheres rapidly reaches convergence for a relatively low order of the expansion. In fact, no further significant decrease in RRMSE is achieved for $N > 7$. On the contrary, if a single radial distance is used to train the model, the corresponding error keeps decreasing up to $N = 20$, but the RRMSE and RRMSE_i on the other spheres remain higher. This is expected since training the equivalent source model with points positioned at a single radial distance does not give to the model any hint on the radial propagation of the acoustic perturbation. Despite the high complexity of the noise generation mechanism considered in this test case (due to the disruptive and constructive interference that may occur between the noise radiated by each rotor), the level of agreement between the reference acoustic fields and the reconstructed one is more than satisfactory, see Fig. 9 obtained with points at $r_{m_{1-3}}$. Visualizations of the results obtained with a training set limited to points at r_{m_1} or r_{m_3} are presented in the Supplementary Information. The plateau in the RRMSE shown in Fig. 8 is a symptom of the presence in the reference acoustic field of components that can't be

Table 2
Propeller geometrical characteristics.

No. of blades, N_b	8, evenly spaced
Chord, c	0.36 m
Angular velocity, ω	2125 rpm
Blade root, r_0	0.124 m
Diameter, d	1.8 m
Blade taper ratio, λ	1.0
Blade airfoil	NACA 65A010

reproduced by the multipolar expansion, or in other words, part of the signal does not correlate with the multipolar sources and their propagation characteristics. Since the multipoles are a base for the acoustic field, the residual error can be interpreted as the presence of numerical noise in the reference signal, or the existence of noise propagation mechanism not correctly addressed by the base: for example, the presence of Doppler effect due to the advancing and retroceding motion of the rotating blades of the rotors is not addressed by the formulation presented in this paper. This phenomenon was not as relevant in the HART II test case as in the quadcopter: in the former, the dominating noise source was the blade vortex interaction, which is "frozen" in space since the blades impact the wake in almost the same positions during successive revolutions.

3.2.3. *Propeller in forward flight*

The configuration here considered is a propeller in forward flight, with an advancing velocity corresponding to $M = 0.5$. The main geometrical characteristics are summarized in Table 2. More information on geometry can be found in [36]. In this case, the model is capable of reproducing the SPL field with satisfactory accuracy, especially in the maximum directivity directions, as shown in Fig. 10 (it is beneficial to train the model using the absolute value of the pressure perturbations on points at various radial distances, as shown in Fig. 12). On the contrary, it is unable to capture the phase of the signal, as demonstrated by Fig. 11, which depicts the real parts of the pressure signal (imaginary parts are not shown for the sake of conciseness). The same considerations made for the quadrotor in hovering may be replied here. Part of the signal and its propagation cannot be reproduced by the multipolar expansion, leading to an incorrect reproduction of the phase fronts. When using only the r_{m_1} sphere in the training set, the solution adheres perfectly to the reference field at the corresponding radial distance, correctly reproducing not only the SPL but also the contribution of the real and imaginary parts of the signal. However, the solution does not follow the phase front modification through radial propagation. On the contrary, when the $r_{m_{1-3}}$ spheres are used in the training set, the model tries to find a solution that fits all three radial distances. However, the radial propagation of the model cannot follow the reference data, and

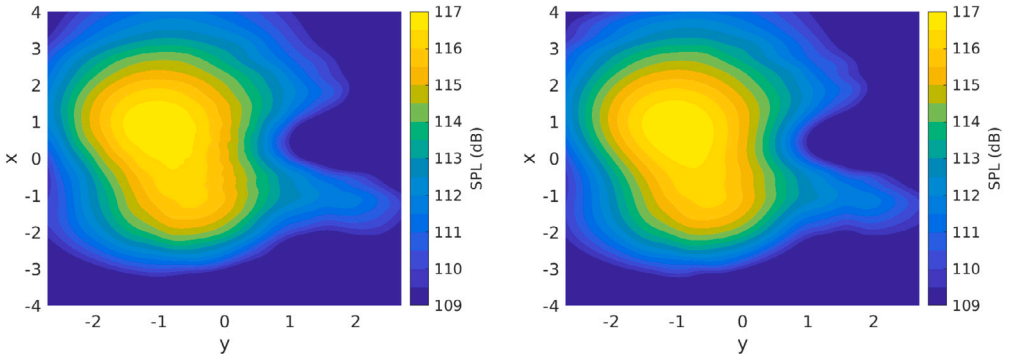

(a) 1 BPF - multipolar expansion

(b) 1 BPF - reference

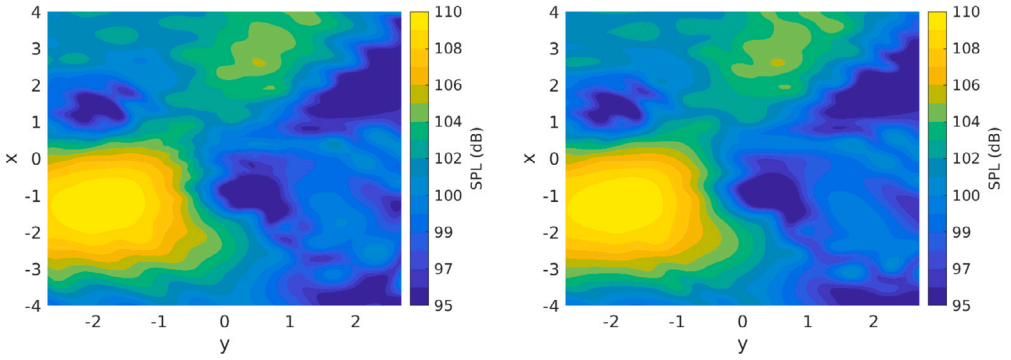

(c) 2 BPF - multipolar expansion

(d) 2 BPF - reference

Fig. 7. Comparison between reconstructed (Fig. 7a, and 7c), and reference (Fig. 7b, and 7d) sound pressure levels for the HART II test case for the first two BPFs, for $N = 20$.

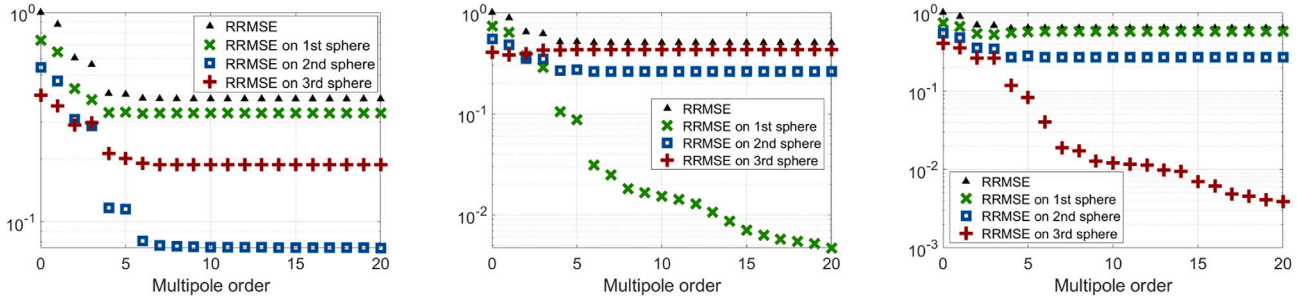

(a) Spheres of radii $r_{m_{1-3}}$ in the training set.

(b) Sphere of radius r_{m_1} in the training set.

(c) Sphere of radius r_{m_3} in the training set.

Fig. 8. Convergence of the normalized RRMSE for the quadcopter in hovering test case.

a compromise solution is obtained that does not match the real and imaginary part at any of the monitoring points but only the absolute values.

4. Conclusion

The authors demonstrated that the analytical expansion of noise fields through multipoles is a viable approach to obtaining equivalent sources of complex acoustic fields when high-fidelity (CAA/CFD) tools are too computationally demanding and low-fidelity semi-empirical models are not available or sufficiently accurate in evaluating noise field due to their limitations. This includes (innovative) aircraft conceptual design, trajectory optimization, and online noise annoyance estimation, and it is also suitable to be included as a source in scattering problems, which is a useful technique when, e.g., an aeroacoustic analysis must be carried out considering the shielding/reflecting effect of the fuselage/wing on an existing engine noise. Once the noise field has been computed or measured at a sufficient number of points, the process of evaluating the equivalent multipoles is practically instantaneous, being based on a simple linear system solution. For best results, the training set points should be placed at different distances from the real source/emitting body and surrounding it (*e.g.*, they can be placed on spheres having different radii). The technique is capable of interpolating and extrapolating noise, and, notably, extrapolation is also possible in the near field. When the order of the expansion is increased, the error has a monotonous decreasing trend, although a relatively small residual error is persistent. Thus, the method was demonstrated to be robust, not only with respect to its order but also with respect to the number of

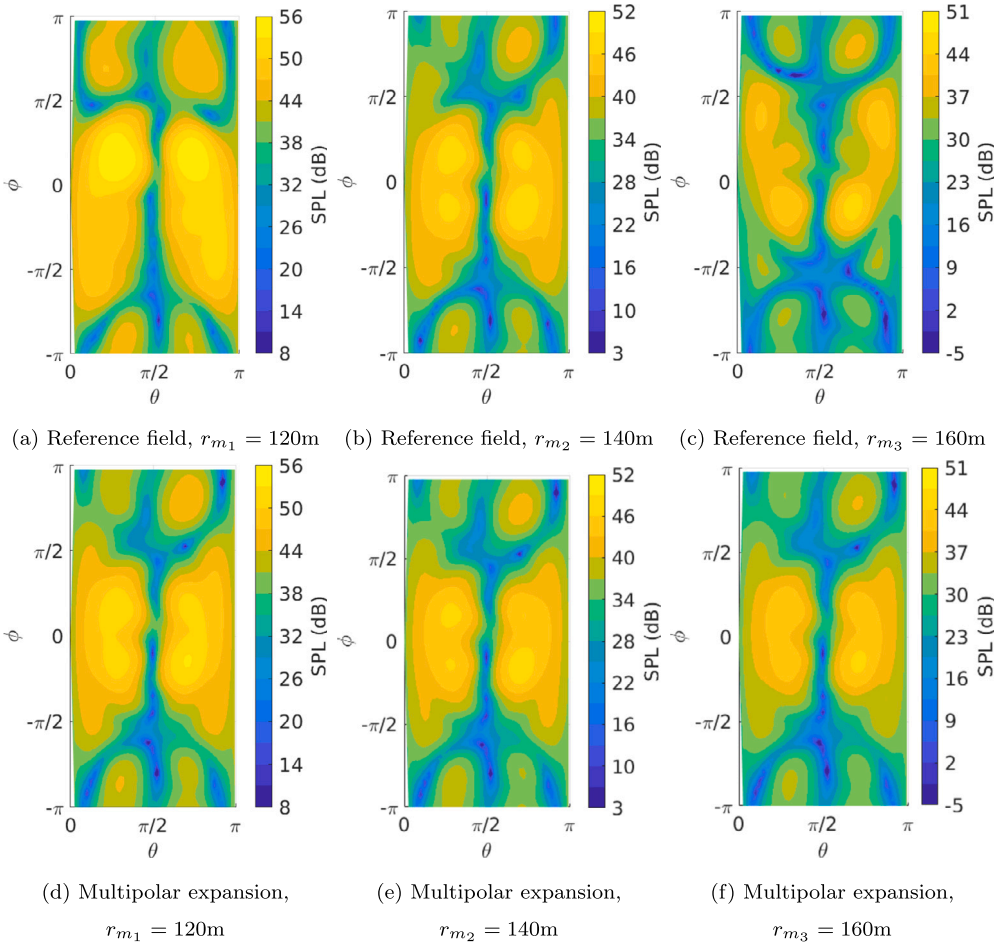

(a) Reference field, $r_{m_1} = 120$m (b) Reference field, $r_{m_2} = 140$m (c) Reference field, $r_{m_3} = 160$m

(d) Multipolar expansion, $r_{m_1} = 120$m (e) Multipolar expansion, $r_{m_2} = 140$m (f) Multipolar expansion, $r_{m_3} = 160$m

Fig. 9. Comparison between reference ((a), (b) and (c)) and reconstructed ((d), (e) and (f)) sound pressure levels at the three radial distances considered, using points at $r_{m_{1-3}}$ in the training set.

points in the training set and their location. The method fails to predict the correct variation of the phase with the observer distance, whereas the absolute value and its propagation are still fairly reproduced when the noise is dominated by the propagation of a rotating source. This suggests the possibility of developing an analytical solution for orbiting multipolar sources in the approximation.

CRediT authorship contribution statement

Giorgio Palma: Writing – review & editing, Writing – original draft, Visualization, Validation, Software, Methodology, Investigation, Formal analysis, Conceptualization. **Lorenzo Burghignoli:** Writing – review & editing, Methodology, Investigation, Conceptualization. **Caterina Poggi:** Writing – review & editing, Writing – original draft, Software, Investigation. **Jacopo Serafini:** Writing – review & editing, Writing – original draft, Supervision, Methodology, Investigation, Conceptualization.

Declaration of competing interest

The authors declare that they have no known competing financial interests or personal relationships that could have appeared to influence the work reported in this paper.

Data availability

Data will be partially made available on request.

Appendix A

Using a cartesian frame of reference, the pressure fields produced by the three linear quadrupoles are described by:

$$\begin{aligned}
\mathcal{P}_{2_{1,1}}(\mathbf{x}) &= \frac{e^{-i\kappa r}}{4\pi r^3}\left[-(1+i\kappa r)+(3+3ir\kappa-r^2\kappa^2)\cos^2\theta\right] \\
\mathcal{P}_{2_{2,2}}(\mathbf{x}) &= \frac{e^{-i\kappa r}}{4\pi r^3}\left[-(1+i\kappa r)+(3+3ir\kappa-r^2\kappa^2)\cos^2\phi\right] \\
\mathcal{P}_{2_{3,3}}(\mathbf{x}) &= \frac{e^{-i\kappa r}}{4\pi r^3}\left[-(1+i\kappa r)+(3+3ir\kappa-r^2\kappa^2)\cos^2\psi\right]
\end{aligned} \tag{A.1}$$

where θ, ϕ and ψ are the angles defining the directional cosines of the direction identified by $\mathbf{r}\cdot\mathbf{e}_1$, $\mathbf{r}\cdot\mathbf{e}_2$ and $\mathbf{r}\cdot\mathbf{e}_3$, respectively. Summing the three terms and recalling that $\cos^2\theta+\cos^2\phi+\cos^2\psi=1$ by definition, one obtains:

$$\mathrm{Tr}\left(\mathcal{P}_2\right) = \frac{e^{-i\kappa r}}{4\pi r^3}\left[-3(1+i\kappa)+\left(3+3i\kappa r-\kappa^2 r^2\right)\right] = \frac{-\kappa^2 e^{-i\kappa r}}{4\pi r^3} \tag{A.2}$$

Using the same procedure is easy to demonstrate that summing $\mathcal{P}_{3_{1,j,j}}$, $\mathcal{P}_{3_{2,j,j}}$, and $\mathcal{P}_{3_{3,j,j}}$, one obtains the three terms $\mathcal{P}_{1_1}$, $\mathcal{P}_{1_2}$ and $\mathcal{P}_{1_3}$, respectively, multiplied by $-\kappa^2$. A general formula may be identified as

$$\mathcal{P}_{n a_1,..,a_n} = \sum_{j=1}^{3} \mathcal{P}_{(n+2)a_1,..,a_n,j,j} \tag{A.3}$$

The multipolar approximation coefficients can be obtained using only the acoustic sources that are components of the two highest-order tensors, ensuring that the matrix $\mathbf{V}$ has full rank.

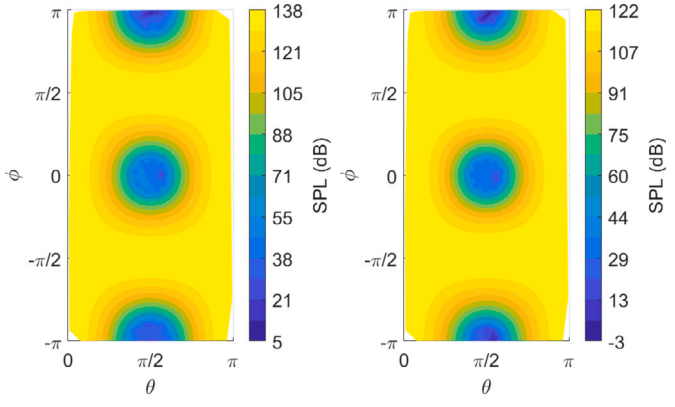

(a) Reference field, $r_{m_1} = 2$m (b) Reference field, $r_{m_3} = 10$m

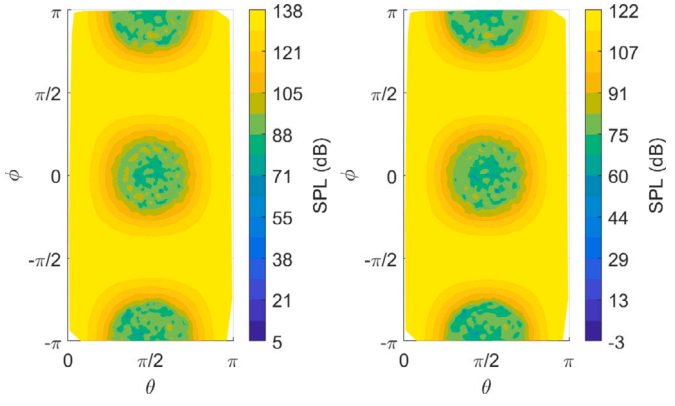

(c) Multipolar expansion, sphere of radius r_{m_1} in the training set with complex signal, $r_{m_1} = 2$m (d) Multipolar expansion, sphere of radius r_{m_1} in the training set with complex signal, $r_{m_3} = 10$m

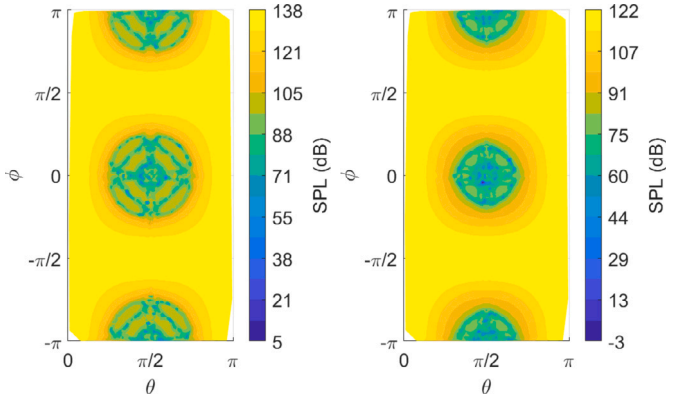

(e) Multipolar expansion, spheres of radii $r_{m_{1-3}}$ in the training set with the absolute value of the signal, $r_{m_1} = 2$m (f) Multipolar expansion, spheres of radii $r_{m_{1-3}}$ in the training set with the absolute value of the signal, $r_{m_3} = 10$m

Fig. 10. Comparison between reference and reconstructed SPL for the BPF of the propeller test case at the three radial distances considered, with different training sets, $n = 20$.

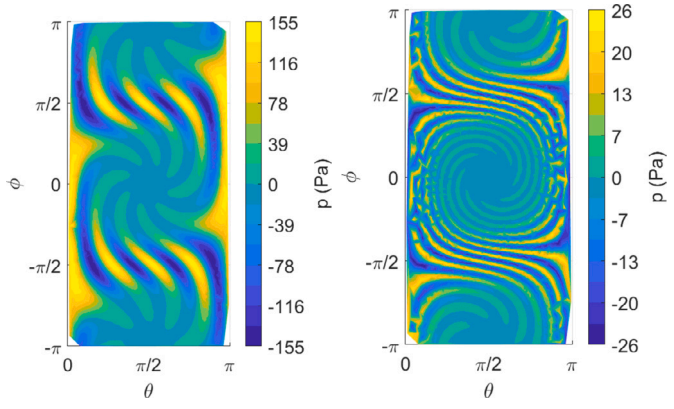

(a) Reference field, $r_{m_1} = 2$m (b) Reference field, $r_{m_3} = 10$m

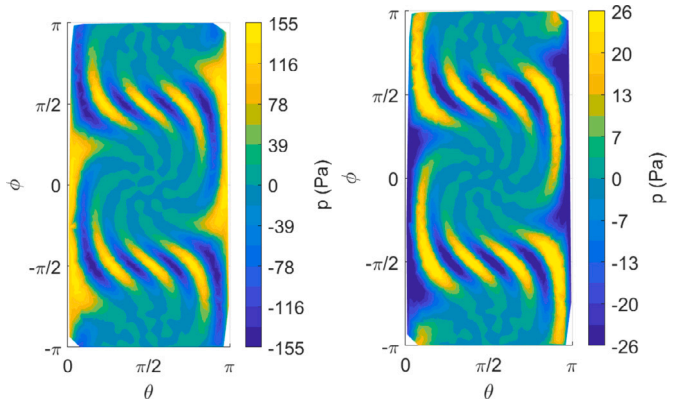

(c) Multipolar expansion, sphere of radius r_{m_1} in the training set, $r_{m_1} = 2$m (d) Multipolar expansion, sphere of radius r_{m_1} in the training set, $r_{m_3} = 10$m

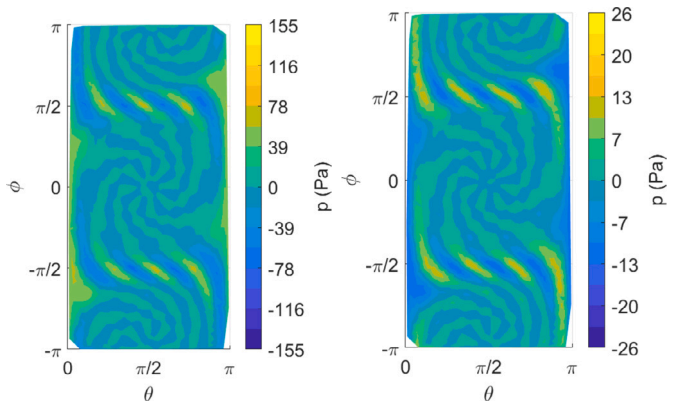

(e) Multipolar expansion, spheres of radii $r_{m_{1-3}}$ in the training set, $r_{m_1} = 2$m (f) Multipolar expansion, spheres of radii $r_{m_{1-3}}$ in the training set, $r_{m_3} = 10$m

Fig. 11. Comparison between reference and reconstructed real part of the acoustic pressures for the BPF of the propeller test case at the three radial distances considered, with different training sets, $n = 20$.

Once the coefficients are evaluated, it is also possible to obtain a description of the expansion in terms of all orders up to N, *i.e.,* to calculate the lower-order coefficients starting from the vector **x**. This has to be done recursively, starting from the highest order. The three terms identified by the right-hand side of Eq. (A.3) should be purged of their average value; the latter becomes the complex-valued amplitude of the term identified by the left-hand side of the same equation. This can be repeated down to the monopolar term.

Appendix B. Supplementary material

Supplementary material related to this article can be found online at https://doi.org/10.1016/j.ast.2024.109629.

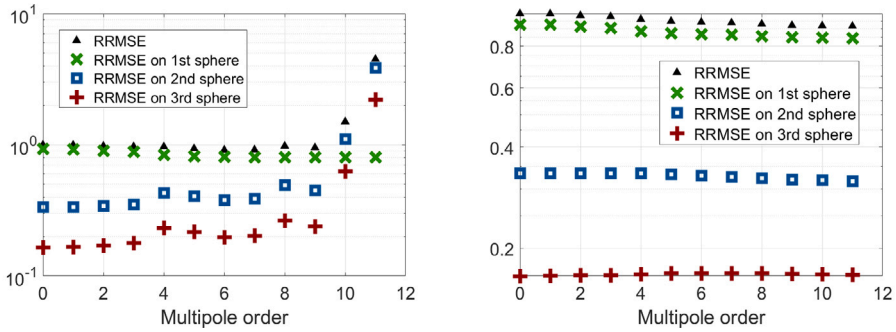

(a) Complex valued pressure on points in sphere r_{m_1} in the training set.

(b) Complex valued pressure on points in spheres $r_{m_{1-3}}$ in the training set.

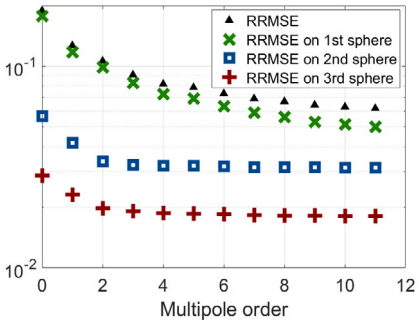

(c) Absolute valued pressure on points in spheres $r_{m_{1-3}}$ in the training set.

Fig. 12. Convergence of the normalized RRMSE, see Eq. (15), for the advancing propeller test case using different training sets.

References

[1] S. Morrell, R. Taylor, D. Lyle, A review of health effects of aircraft noise, Aust. N. Z. J. Public Health 21 (2) (1997) 221–236.

[2] E. Commission, D.-G. for Mobility, Transport, D.-G. for Research, Innovation, Flightpath 2050 – Europe's vision for aviation – Maintaining global leadership and serving society's needs, Publications Office, 2011.

[3] Environment and energy research and development @ Policy, International Affairs and Environment, http://www.faa.gov.

[4] ICAO, Environment giacc–4, Tech. Rep., International Civil Aviation Organization, 2012.

[5] I. C. A. Organization, Guidance on the balanced approach to aircraft noise management, vol. 9829, International Civil Aviation Organization, 2008.

[6] J.-P. Clarke, The role of advanced air traffic management in reducing the impact of aircraft noise and enabling aviation growth, in: Aviation and Sustainability, J. Air Transp. Manag. 9 (3) (2003) 161–165, https://doi.org/10.1016/S0969-6997(02)00080-7.

[7] S. Mendez, M. Shoeybi, S. Lele, P. Moin, On the use of the ffowcs Williams-Hawkings equation to predict far-field jet noise from large-eddy simulations, Int. J. Aeroacoust. 12 (1–2) (2013) 1–20.

[8] M. Gennaretti, L. Luceri, L. Morino, A unified boundary integral methodology for aerodynamics and aeroacoustics of rotors, J. Sound Vib. 200 (4) (1997) 467–489.

[9] A.S. Lyrintzis, Review: the use of Kirchhoff's method in computational aeroacoustics, J. Fluids Eng. 116 (4) (1994) 665–676, https://doi.org/10.1115/1.2911834, https://asmedigitalcollection.asme.org/fluidsengineering/article-pdf/116/4/665/5717371/665_1.pdf.

[10] J. Prieur, G. Rahier, Aeroacoustic integral methods, formulation and efficient numerical implementation, Aerosp. Sci. Technol. 5 (7) (2001) 457–468.

[11] G. Spencer, M. Murty, General ray-tracing procedure, J. Opt. Soc. Am. A 52 (6) (1962) 672–678.

[12] J.F. Harindra, Handbook of Environmental Fluid Dynamics, Volume Two: Systems, Pollution, Modeling, and Measurements, CRC Press, 2018.

[13] R. Pieren, L. Bertsch, D. Lauper, B. Schäffer, Improving future low-noise aircraft technologies using experimental perception-based evaluation of synthetic flyovers, Sci. Total Environ. 692 (2019) 68–81.

[14] S. Lee, Review: the use of equivalent source method in computational acoustics, J. Comput. Acoust. 25 (01) (2017) 1630001, https://doi.org/10.1142/S0218396X16300012.

[15] F. Holste, An equivalent source method for calculation of the sound radiated from aircraft engines, J. Sound Vib. 203 (4) (1997) 667–695, https://doi.org/10.1006/jsvi.1996.0891.

[16] G. Pavi, A technique for the computation of sound radiation by vibrating bodies using multipole substitute sources, Acta Acust. Acust. 92 (1) (2006) 112–126.

[17] B. Treeby, F. Lucka, E. Martin, B.T. Cox, Equivalent-source acoustic holography for projecting measured ultrasound fields through complex media, IEEE Trans. Ultrason. Ferroelectr. Freq. Control 65 (10) (2018) 1857–1864, https://doi.org/10.1109/TUFFC.2018.2861895.

[18] G.F. Pinton, J. Dahl, S. Rosenzweig, G.E. Trahey, A heterogeneous nonlinear attenuating full-wave model of ultrasound, IEEE Trans. Ultrason. Ferroelectr. Freq. Control 56 (3) (2009) 474–488.

[19] B.E. Treeby, J. Jaros, A.P. Rendell, B.T. Cox, Modeling nonlinear ultrasound propagation in heterogeneous media with power law absorption using a k-space pseudospectral method, J. Acoust. Soc. Am. 131 (6) (2012) 4324–4336, https://doi.org/10.1121/1.4712021, https://pubs.aip.org/asa/jasa/article-pdf/131/6/4324/15298882/4324_1_online.pdf.

[20] Y. Xu, W. Xue, Y. Li, L. Guo, W. Shang, Electromagnetic field analysis of an electric dipole antenna based on a surface integral equation in multilayered dissipative media, Appl. Sci. 7 (8) (2017).

[21] D.A. Russell, On the sound field radiated by a tuning fork, Am. J. Phys. 68 (12) (2000) 1139–1145, https://doi.org/10.1119/1.1286661.

[22] R.E. Musafir, The multipole expansion: a new look, J. Sound Vib. 236 (5) (2000) 904–911, https://doi.org/10.1006/jsvi.2000.3044.

[23] E.G. Williams, Chapter 6 - spherical waves, in: E.G. Williams (Ed.), Fourier Acoustics, Academic Press, London, 1999, pp. 183–234.

[24] D. McNamara, C. Pistorius, J. Malherbe, Introduction to the Uniform Geometrical Theory of Diffraction, Antennas and Propagation Library, Artech House, 1990.

[25] S.L. Denisov, A.I. Korolkov, Investigation of noise-shielding efficiency with the method of sequences of maximum length in application to the problems of aviation acoustics, Acoust. Phys. 63 (4) (2017) 462–477, https://doi.org/10.1134/S1063771017040017.

[26] S.L. Denisov, V.F. Kopiev, N.N. Ostrikov, G.A. Faranosov, S.A. Chernyshev, Using the correlation model of random quadrupoles of sources to calculate the efficiency of turbulent jet noise screening with geometric diffraction theory, Acoust. Phys. 66 (5) (2020) 528–541, https://doi.org/10.1134/S1063771020050024.

[27] M. Despotovic, V. Nedic, D. Despotovic, S. Cvetanovic, Evaluation of empirical models for predicting monthly mean horizontal diffuse solar radiation, Renew. Sustain. Energy Rev. 56 (2016) 246–260, https://doi.org/10.1016/j.rser.2015.11.058.

[28] M. Gennaretti, G. Bernardini, Novel boundary integral formulation for blade-vortex interaction aerodynamics of helicopter rotors, AIAA J. 45 (6) (2007) 1169–1176.
[29] F. Farassat, Derivation of formulations 1 and 1A of farassat, NASA TM-2007-214853, 1979.
[30] B.G. van der Wall, 2nd hhc aeroacoustic rotor test (hart ii)-part i: Test documentation, Tech. Rep., US Army AFDD, NASA Langley, DLR, ONERA and DNW, 2003.
[31] B.G. van der Wall, C.L. Burley, Y. Yu, H. Richard, K. Pengel, P. Beaumier, The hart ii test – measurement of helicopter rotor wakes, Aerosp. Sci. Technol. 8 (4) (2004) 273–284, https://doi.org/10.1016/j.ast.2004.01.001.
[32] B.G. van der Wall, C.L. Burley, 2nd hhc aeroacoustic rotor test (hart ii)-part ii: representative results, Tech. Rep., US Army AFDD, NASA Langley, DLR, ONERA and DNW, 2005.
[33] B.G. van der Wall, J.W. Lim, M.J. Smith, S.N. Jung, J. Bailly, J.D. Baeder, D.D. Boyd, The hart ii international workshop: an assessment of the state-of-the-art in comprehensive code prediction, CEAS Aeronaut. J. 4 (2013) 223–252.
[34] M. Gennaretti, G. Bernardini, J. Serafini, G. Romani, Rotorcraft comprehensive code assessment for blade–vortex interaction conditions, Aerosp. Sci. Technol. 80 (2018) 232–246, https://doi.org/10.1016/j.ast.2018.07.013.
[35] C. Poggi, G. Bernardini, M. Gennaretti, F. Porcacchia, Optimal performance trim procedure for multirotor vertical takeoff and landing vehicles, J. Aircr. (2023) 1–11.
[36] C. Poggi, M. Rossetti, J. Serafini, G. Bernardini, M. Gennaretti, U. Iemma, Neural network meta–modelling for an efficient prediction of propeller array acoustic signature, Aerosp. Sci. Technol. 130 (2022) 107910.